Appl. Phys. B 74 [Suppl.], S231–S236 (2002)
DOI: 10.1007/s00340-002-0889-5

Applied Physics B
Lasers and Optics

K.-H. HONG✉
J.-H. KIM
Y.H. KANG
C.H. NAM

Time–frequency analysis of chirped femtosecond pulses using Wigner distribution function

Department of Physics & Coherent X-ray Research Center, Korea Advanced Institute of Science and Technology, 373-1 Gusong-dong, Yusong-gu, Daejoen 305-701, Korea

Received: 18 September 2001/
Revised version: 12 November 2001
Published online: 20 June 2002 •

ABSTRACT A time–frequency analysis of chirped femtosecond pulses using the Wigner distribution function is presented. We graphically obtain the instantaneous carrier frequency and the group delay of the chirped pulse using a peak-detection method. After confirming that the instantaneous carrier frequency of an ultra-short laser pulse defined by the derivative of the temporal phase is not generally supported by the optical frequency, we use the Wigner distribution to decompose the optical frequencies that mainly contribute to the pulse at a certain time. For this purpose, a chirped pulse with a double-peaked spectrum and one whose phase is distorted by third-order dispersion are analyzed with the peak-detection method. The Wigner distribution along with this graphical method successfully resolves the multicomponent frequencies that cannot be seen in the standard Fourier analysis.

PACS 42.30.Rx; 42.65.Re

1 Introduction

The time-dependent phase is one of the crucial parameters to precisely represent the characteristics of an ultra-short laser pulse, especially in the femtosecond regime. Due to the broad spectrum, the spectral intensity or spectral phase of ultra-short laser pulses is easily influenced by optical elements such as a gain medium, glass block, prism, and grating. The frequency chirp induced by material or angular dispersion, and the spectral filtering by an etalon effect, are good examples of such modulation. Any modification in either the spectral intensity or the spectral phase of laser pulses directly affects the temporal intensity and phase. The temporal phase measurements by recently developed techniques, such as frequency-resolved optical gating (FROG) [1] and spectral phase interferometry for direct electric-field reconstruction (SPIDER) [2], show that femtosecond pulses do not usually have a constant phase in time.

The nonlinear dependence on time of a phase implies the existence of a time-dependent carrier frequency. The relation between these two quantities is given by $\omega(t) = \omega_0 - (\mathrm{d}\varphi/\mathrm{d}t)$, where ω_0 is the center frequency, $\omega(t)$ is the time-dependent carrier frequency, and φ is the temporal phase. This time-dependent carrier frequency $\omega(t)$ is usually called the 'instantaneous (carrier) frequency' of the pulse, meaning the carrier frequency at time t. We can quantitatively analyze the amount of laser chirp using this relationship after measuring the temporal phase. However, this interpretation sometimes fails because this quantity does not generally coincide with the Fourier spectral component at time t [3].

Recently, efforts to properly interpret the 'instantaneous frequency' have been made in the analysis of frequency-modulated (FM) and amplitude-modulated (AM) signals containing multiple frequency components [4–6]. However, a study of the problem of the interpretation of the instantaneous (carrier) frequency of an ultra-short laser pulse has not been reported yet.

Time–frequency distribution functions are appropriate tools to interpret the instantaneous carrier frequency, because they can simultaneously describe the temporal and spectral behavior of ultra-short laser pulses by revealing time-resolved spectral structure, whereas standard Fourier analysis shows only the averaged information in the time and frequency domain. The Wigner distribution (WD) has the simplest form among the usually used time–frequency distribution functions [7] and has a good marginal property. The WD of an ultra-short laser pulse can display features that bear a close relation to the instantaneous carrier frequency and group delay of the pulse, which makes it possible to analyze the laser chirp quantitatively. For these reasons, adopted as a tool for the description of ultra-short pulses [8], it has been applied to the measurement of amplitude and phase of ultra-short laser pulses [9, 10] and the analysis of the error criteria of pulse-characterization techniques [11]. The WD also played a significant role in the analysis of a complicated structure of high-order harmonics generated by intense ultra-short pulses [12] and in the representation of quantum particles in phase space [13].

This paper is organized as follows. In Sect. 2, we describe the time–frequency structure of a chirped Gaussian pulse using the WD. The instantaneous carrier frequency and group delay are quantitatively analyzed using a peak-detection method [14] in the WD. In Sect. 3, we present a time–frequency analysis of two types of pulses – a chirped pulse with a double-peaked spectrum and a high-order chirped pulse distorted by third-order dispersion (TOD) – whose instantaneous carrier frequency cannot be directly interpreted in

✉ Fax: +82-42/869-2510, E-mail: pman@bomun.kaist.ac.kr

terms of the optical or Fourier spectrum. Sect. 4 is devoted to the time–frequency analysis of experimentally measured femtosecond chirped pulses from a chirped-pulse amplification (CPA) laser. An experimentally measured pulse whose phase is distorted by TOD is also analyzed using the WD. In Sect. 5, we summarize the results and make conclusions.

2 Wigner distribution for a chirped Gaussian pulse

The WD for the electric field in the time domain, $E(t)$, is defined as

$$W(t,\omega)=\frac{1}{\pi}\int_{-\infty}^{+\infty}E\left(t+\frac{1}{2}t'\right)E^{*}\left(t-\frac{1}{2}t'\right)\exp(-\mathrm{i}\omega t')\mathrm{d}t'. \tag{1}$$

An equivalent definition is possible using the electric field in the frequency domain, $\tilde{E}(\omega)$, and is written as

$$W(t,\omega)=\frac{1}{\pi}\int_{-\infty}^{+\infty}\tilde{E}^{*}\left(\omega+\frac{1}{2}\omega'\right)\tilde{E}\left(\omega-\frac{1}{2}\omega'\right)\exp(-\mathrm{i}\omega' t)\mathrm{d}\omega'. \tag{2}$$

The usefulness of this representation comes mainly from its good marginal property: the time marginal defined by the integration along the ω axis represents the intensity profile, and the frequency marginal, the integration along the t axis, gives the spectral profile. Thus, this representation directly expresses how the carrier frequency changes with the time evolution of the pulse and how the group delay varies with the laser frequency. For a quantitative time–frequency analysis of the laser chirp, two parameters, linear chirp parameter and group-delay dispersion (GDD), are important. The linear chirp parameter is given by the second derivative of the temporal phase at time zero with minus sign or $\alpha=-\mathrm{d}^2\varphi/\mathrm{d}t^2|_{t=0}$, and the GDD is calculated by the second derivative of the spectral phase at the center frequency or $\beta=\mathrm{d}^2\tilde{\varphi}/\mathrm{d}\omega^2|_{\omega=\omega_0}$. The linear chirp parameter and the GDD represent the variation of the instantaneous carrier frequency and the group delay, respectively.

For a linearly chirped pulse with a single frequency component, the instantaneous carrier frequency and group delay can be directly obtained from the WD by the local average concept. For an arbitrary pulse $E(t)=A(t)\,\mathrm{e}^{\mathrm{i}\{\omega_0 t-\varphi(t)\}}$, the frequency averaged at time t is given by the following relation [15]:

$$\begin{aligned}\langle\omega\rangle_t &\equiv \frac{\int_{-\infty}^{\infty}\mathrm{d}\omega W(t,\omega)\omega}{\int_{-\infty}^{\infty}\mathrm{d}\omega W(t,\omega)}\\ &=\omega_0-\frac{\mathrm{d}\varphi(t)}{\mathrm{d}t} \qquad (3)\\ &=\omega(t). \qquad (4)\end{aligned}$$

This means that the instantaneous carrier frequency is the frequency average over the WD. Similarly, the time averaged at frequency ω with minus sign, $-\langle t\rangle_\omega$, corresponds to the group delay when it is calculated in the frequency domain.

However, if a pulse contains multiple frequency components, the local average fails to give detailed information about each frequency component. In the simple case of a chirped Gaussian pulse, the energy distribution is localized along the instantaneous carrier frequency in the time domain and the group delay in the frequency domain because of its single-peaked and symmetric structure, and thus the local averages coincide with the WD peaks. In the case of an arbitrary pulse, however, the energy distribution is localized along the WD peaks rather than the local averages. For this reason, the peak-detection method is more useful than the local average calculation to decompose the pulse with a multicomponent spectrum. In this paper, to graphically retrieve the instantaneous carrier frequency and the group delay from the WD, we will use a peak-detection method [14] instead of the local average calculation. We describe this method using a chirped Gaussian pulse and express it graphically. The usefulness of this method is discussed for more general cases in Sect. 3.

When a Gaussian pulse is chirped with the GDD, β, it can be described in the spectral domain as

$$\tilde{E}(\omega)=\mathrm{e}^{-\left(\frac{T_{\mathrm{G0}}}{2}\right)^2(\omega-\omega_0)^2}\mathrm{e}^{\mathrm{i}\frac{\beta}{2}(\omega-\omega_0)^2}, \tag{5}$$

where $T_{\mathrm{G0}}=T_{\mathrm{p}}/\sqrt{2\ln 2}$ and T_{p} is the chirp-free pulse duration in full-width at half maximum (FWHM). By the Fourier-transform relation, the linear chirp parameter α of this pulse is calculated to be

$$\alpha=\frac{4\beta}{T_{\mathrm{G0}}^4+4\beta^2}. \tag{6}$$

At first the linear chirp parameter increases with GDD, and then it decreases due to more rapid pulse broadening. Maximum and minimum linear chirps occur when $\beta=+\frac{T_{\mathrm{G0}}^2}{2}$ and $\beta=-\frac{T_{\mathrm{G0}}^2}{2}$, respectively.

The intensity-normalized Wigner distribution function for the pulse given by (5) is explicitly written as

$$W(t,\omega)=\exp\left[-\frac{2}{T_{\mathrm{G0}}^2}\left(t^2-2\beta\omega t+\frac{T_{\mathrm{G0}}^4+4\beta^2}{4}\omega^2\right)\right]. \tag{7}$$

Figure 1 shows the Wigner distribution for a chirped Gaussian pulse when $\beta=225\ \mathrm{fs}^2$ and $T_{\mathrm{p}}=24$ fs. The Wigner contours are in the shape of ellipses whose major axis (a) is rotated by θ about the ω axis. One may intuitively conceive that the angle θ is quantitatively related to the linear chirp parameter or GDD. However, the time and frequency axes should be properly normalized for this purpose [9, 10] and, moreover, this angle cannot describe the two quantities at a time.

By looking at (7) along with Fig. 1, we can find out how the group delay and instantaneous carrier frequency manifest themselves in the WD. For a given frequency ω, the WD has a maximum at $t_{\max}=\beta\omega$. If ω is scanned across the laser spectrum, these points make a line with a slope β to the ω axis. Because β is the GDD of the chirped pulse, this line represents the group delay. With the same principle, for a fixed time t, the WD is at a maximum when $\omega_{\max}=4\beta/(T_{\mathrm{G0}}^4+4\beta^2)t=\alpha t$. When t is scanned across the pulse, the line connecting the

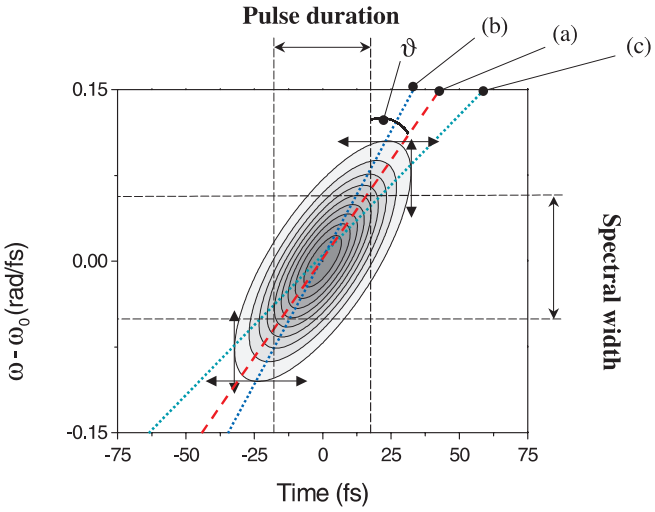

FIGURE 1 Graphical interpretation of the WD of a chirped Gaussian pulse. (a) Major axis of the ellipse formed by Wigner contours, (b) group delay (function of ω), and (c) instantaneous carrier frequency (function of t)

maximum points or WD peaks represents the instantaneous carrier frequency with a slope α, the linear chirp parameter. This peak-detection method is graphically explained in Fig. 1. The group delay and the instantaneous carrier frequency obtained using this method are given by the lines (b) and (c), respectively. In the case where the absolute value of GDD is large or the Wigner contours have a large ellipticity, we can see from (6) that the GDD is inverse to the linear chirp parameter, and that the two lines (b) and (c) in Fig. 1 overlap.

3 Time–frequency analysis of various chirped pulses

In the case of a Gaussian pulse, the instantaneous carrier frequency is well defined within the optical spectrum, so that we can interpret it to be the optical frequency at a certain moment. However, the concept of 'instantaneous carrier frequency' is somewhat contradictory because the frequency is originally defined in the temporal region from $-\infty$ to $+\infty$. In some cases, the instantaneous carrier frequency can be out of the range set by the optical spectrum. An example for this case is given in Fig. 2. It shows the temporal and spectral structure of a chirped femtosecond pulse with a double-peaked spectrum, where the group delay (d) linearly increases with frequency. The instantaneous carrier frequency (b) is beyond the optical spectrum (c) around the valley of the laser intensity profile (a) as indicated by the two arrows. This means that the instantaneous carrier frequency, $\omega(t)$, of an ultra-short laser pulse cannot be interpreted as an optical frequency at time t in general. Other examples having this kind of problem in the case of a discrete spectrum were given in [3, 5].

The main reason for this mismatch between the instantaneous carrier frequency and the optical spectrum is that the pulse has a multipeaked spectrum. Since the multiple frequency components are not decomposed in the Fourier analysis or in the calculation of the local average of the WD, the instantaneous carrier frequency fails to match the optical spectrum. However, the WD in combination with the peak-detection method can decompose these frequency components because the energy is distributed along the WD peaks. We will apply the peak-detection method to two types of pulses to decompose the optical frequencies that mainly contribute at each part of the pulses.

The first case is a chirped pulse with a spectrum double-peaked at $\omega_0 \pm 0.4$ rad/fs, which was already shown in Fig. 2. The WD of this pulse is represented in Fig. 3. Whereas the group delay (c) is linear in the frequency and exactly the same as the line obtained by the peak-detection method, the instantaneous carrier frequency (a) is nonlinear in time and does not remain within the optical spectrum. On the other hand, the optical frequencies decomposed by the peak-detection method are localized within the optical spectrum as represented by (b). The lines (b) consist of three parts, and the temporal shape of the pulse is also composed of three parts. The carrier frequency of $\omega_0 - 0.4$ rad/fs is dominant at the leading sub-pulse, and $\omega_0 + 0.4$ rad/fs at the trailing sub-pulse. At the main part of the pulse, the dominant carrier frequency is

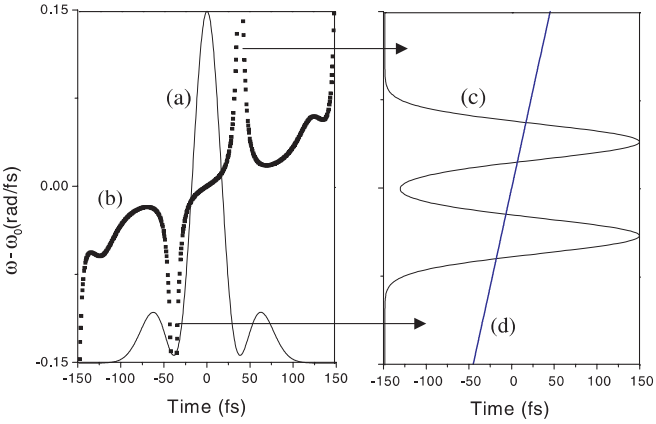

FIGURE 2 Chirped femtosecond pulse with a double-peak spectrum. (a) Temporal intensity profile, (b) instantaneous carrier frequency, (c) spectrum profile, and (d) group delay. The instantaneous carrier frequency is outside the optical spectrum at around $\omega_0 \pm 40$ fs as indicated by two *arrows*

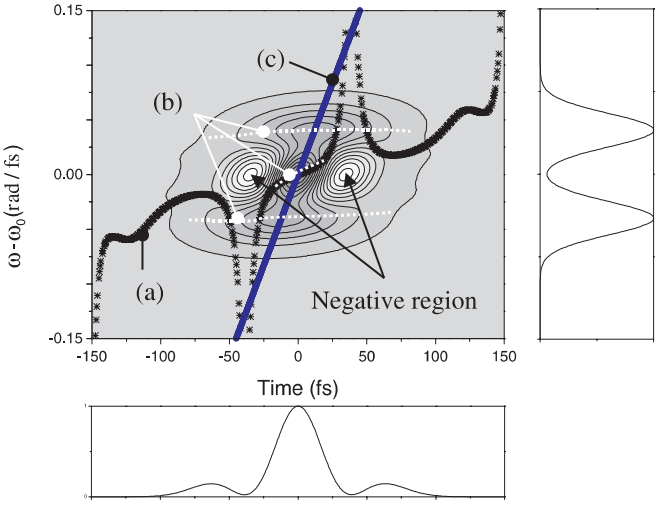

FIGURE 3 Wigner distribution of the chirped pulse with a double-peak spectrum. (a) Instantaneous carrier frequency, (b) decomposed optical frequencies obtained using the peak-detection method, and (c) group delay. The time and frequency marginals are shown at the *bottom* and *right-hand side*

positively chirped around the center frequency ω_0, and the $\omega_0 \pm 0.4$ rad/fs components also exist.

The second case is a chirped pulse whose phase is distorted by TOD or quadratic group delay. The Wigner distribution of a laser pulse distorted by the TOD of 10^4 fs^3 is shown in Fig. 4. The instantaneous carrier frequency (a) is constant throughout the pulse, whereas the optical frequency obtained by the peak-detection method (b) contains two dominant components in the leading part and the same one as (a) in the trailing part. The constant instantaneous carrier frequency can lead us to misunderstand this pulse, but the WD gives us clear information about the mixed frequencies contained in the pulse. The group delay deviation between the given curve (c) and that obtained by the peak-detection method (d) is due to the existence of the negative region of the WD values in the leading part. We can observe that the peak position of the pulse (the group delay value at ω_0) is determined by the curve (d) rather than (c) as shown in the intensity profile and, as a result, it comes before $t = 0$ rather than at $t = 0$. This means that (d) is meaningful for the main part of the pulse.

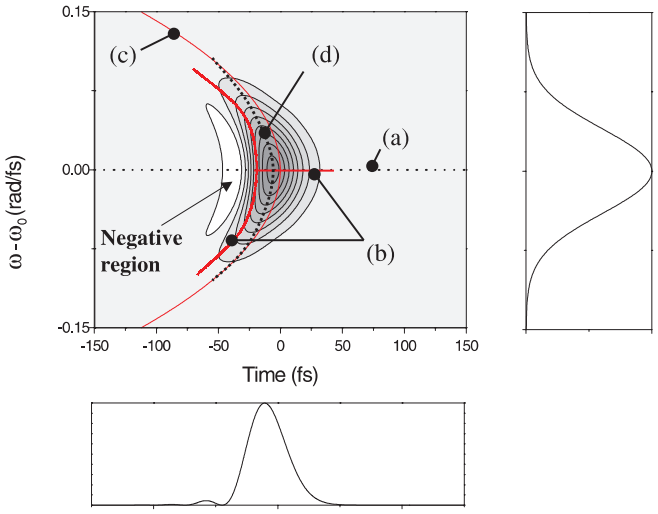

FIGURE 4 Wigner distribution of a chirped pulse distorted by TOD. (a) Instantaneous carrier frequency, (b) decomposed optical frequencies obtained using the peak-detection method, (c) given group delay, and (d) group delay obtained using the peak-detection method. The time and frequency marginals are shown at the *bottom* and *right-hand side*. The instantaneous optical frequency is decomposed into two parts in the leading edge of the pulse

4 Time–frequency analysis of experimentally measured optical pulses

Chirped femtosecond pulses are easily generated in a CPA laser by the dispersion control of a pulse compressor. The GDD of the laser pulses varies depending on the grating separation of the pulse compressor without changing the spectrum. We generated various chirped pulses from a CPA Ti:sapphire laser [16] by adjusting the grating separation of the pulse compressor, which consists of two 1200-groove/mm gratings and a retro-reflector. The incident angle of the laser beam to the first grating was 46°, and the grating separation was changed along the direction of laser incidence. The grating separation at which the GDD is zero or a *chirp-free* pulse is generated was set to be the zero grating position. The grating separation was scanned from -500 μm to $+500$ μm with regard to the zero grating position. The electric field was characterized using a single-shot second-harmonic-generation FROG apparatus. The convergence of the FROG algorithms (called the FROG error) after the reconstruction of the electric fields was 0.004. The electric fields so obtained were substituted for $E(t)$ in (1) to give the WD for the time–frequency analysis.

Figure 5 shows the WD of positively and negatively chirped pulses generated in the CPA laser. The GDD linearly decreases as the grating separation increases, and the sign of the GDD determines the direction of the laser chirp. Figure 5a to c show positively chirped pulses generated by the insufficient dispersion compensation of the pulse compressor, whereas Fig. 5e to g show negatively chirped pulses produced by overcompensation of the dispersion. Figure 5d

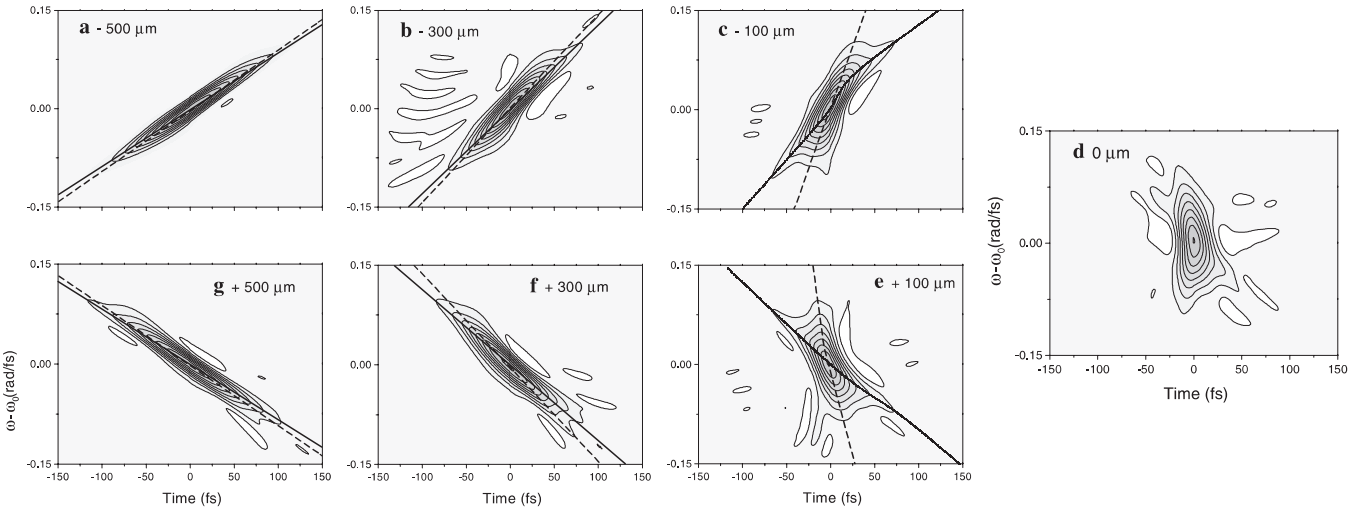

FIGURE 5 The WD of chirped femtosecond pulses generated by the dispersion control of a CPA laser. The grating separation was scanned along the laser incidence direction from -500 μm (**a**) to $+500$ μm (**g**) with regard to the zero grating separation in which the *chirp-free* pulse is generated (**d**) . The incidence angle to the grating with the groove number of 1200 lines/mm was 46°. The instantaneous carrier frequencies and group delays obtained using the peak-detection method are represented by the *solid* and *dashed lines*, respectively

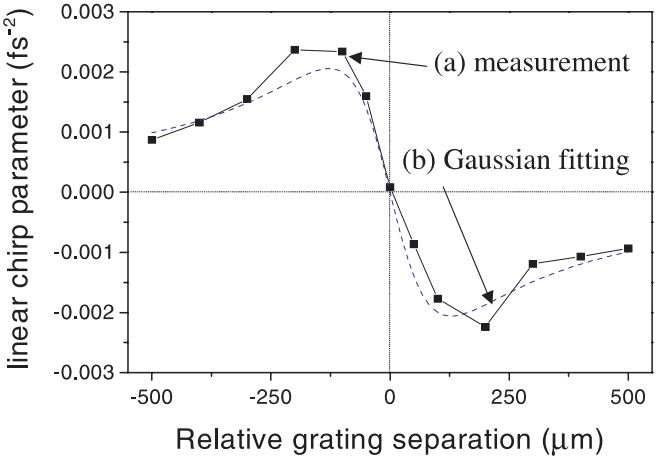

FIGURE 6 The linear chirp parameter (the slope of the instantaneous carrier frequency) as a function of the relative grating separation. (a) Linear chirp parameter of the chirped femtosecond pulses generated in the CPA laser and (b) fitted curve for the Gaussian case

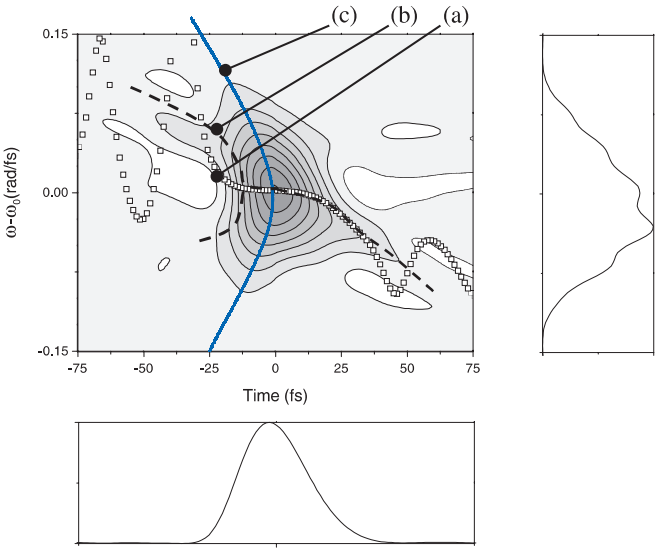

FIGURE 7 Wigner distribution of experimentally measured pulse distorted by TOD. (a) Instantaneous carrier frequency, (b) decomposed optical frequencies, and (c) group delay obtained using the peak-detection method. The time and frequency marginals are shown at the *bottom* and *right-hand side*

shows the pulse with zero GDD, obtained at zero grating separation. All the pulses have the same spectrum (frequency marginal) but with different temporal intensity profiles (time marginal). The pulse-broadening effect by the GDD is clearly seen. The peak-detection method was applied to analyze the laser chirp of the measured pulses, which allows one to simultaneously see the instantaneous carrier frequency and the group delay of the femtosecond chirped pulses. The instantaneous carrier frequency and the group delay lines coincide with each other at the large grating separation as seen in Fig. 2a and g; in this case, the linear chirp parameter and the GDD are simply inverse to each other as mentioned in Sect. 2. The change of the linear chirp parameter as a function of the grating separation is shown in Fig. 6. It was fitted to the Gaussian curve given by (6). This curve implies that a large GDD does not always increase the slope of the instantaneous carrier frequency.

The pulse whose phase is distorted by TOD can also be observed in a CPA laser when the grating compressor is not optimized for the compensation of high-order dispersion terms. Figure 7 shows the WD of an experimentally measured femtosecond pulse with a zero GDD that appeared in Fig. 5d. Figure 7a shows the instantaneous carrier frequency, and Fig. 7b shows the optical frequencies obtained by the peak-detection method. The quadratic group delay (Fig. 7c) obtained using the peak-detection method shows that TOD remains in the pulse, and thus this pulse exhibits a feature similar to that shown in Fig. 4. There exist multicomponent frequencies in the leading part of the pulse, too.

5 Summary and conclusions

A time–frequency analysis using the WD has been applied to a variety of chirped pulses. For a graphical interpretation of the instantaneous carrier frequency and the group delay of a chirped Gaussian pulse in the Wigner time–frequency distribution, we used the peak-detection method rather than the calculation of the local average or the derivative of the temporal phase. We characterized the chirped femtosecond pulses generated in a CPA laser using the FROG technique and represented the retrieved pulses in the time–frequency domain using the WD. The instantaneous carrier frequency and the group delay of the chirped pulses were graphically obtained using the peak-detection method. We have found that, as the GDD (the slope of the group delay) linearly increases from zero, the linear chirp parameter (the slope of the instantaneous carrier frequency) increases with the GDD, and after attaining a maximum it decreases. For a large GDD, the linear chirp parameter becomes the inverse of the GDD.

The instantaneous carrier frequency defined by $\omega(t) = \omega_0 - (\mathrm{d}\varphi/\mathrm{d}t)$ sometimes fails to give a proper physical interpretation. By showing an example in which the pulse has a double-peaked spectrum, we confirmed that this quantity is not always supported by the optical frequency at time t in a laser pulse. We applied the peak-detection method to decompose the optical frequencies that mainly contribute at time t, which can be resolved neither by the local average calculation nor by the standard Fourier analysis. The laser pulse whose phase is distorted by TOD also has an interesting time–frequency structure. The peak-detection method graphically resolved the two dominant optical frequency components in the leading part of this pulse. An experimentally measured pulse whose phase is distorted by TOD was also analyzed. In conclusion, the time–frequency analysis along with the graphical interpretation using the peak-detection method helped us to understand the instantaneous carrier frequency, the group delay, and the corresponding laser chirp of an ultra-short laser pulse.

ACKNOWLEDGEMENTS This work is supported by the Ministry of Science and Technology of Korea through the Creative Research Initiative Program.

REFERENCES

1 B. Kohler, V.V. Yakovlev, K.R. Wilson, J. Squiffer, K.W. DeLong, R. Trebino: Opt. Lett. **20**, 483 (1995)
2 C. Dorrer, B. de Beauvoir, C. Le Blanc, J.-P. Rousseau, S. Ranc, P. Rousseau, J.-P. Chambaret, F. Salin: Opt. Lett. **24**, 1644 (1999)
3 L. Mandel: Am. J. Phys. **42**, 840 (1974)
4 B. Ristic, B. Boashash: IEEE Trans. Signal Proc. **44**, 1549 (1996)
5 P.J. Loughlin: IEEE Signal Proc. Lett. **4**, 123 (1997)
6 W. Nho, P.J. Loughlin: IEEE Signal Proc. Lett. **6**, 78 (1999)
7 L. Cohen: Proc. IEEE **77**, 941 (1989)
8 J. Paye: IEEE J. Quantum Electron. **QE-28**, 2262 (1992)
9 R. Gase: J. Opt. Soc. Am. B **14**, 2915 (1997)
10 I.A. Walmsley, V. Wong: J. Opt. Soc. Am. B **13**, 2453 (1996)
11 S. Yeremenko, A. Baltuska, M.S. Pshenichnikov, D.A. Wiersma: Appl. Phys. B **70**, S109 (2000)
12 J.-H. Kim, D.G. Lee, H.J. Shin, C.H. Nam: Phys. Rev. A **63**, 063 403 (2001)
13 E. Wigner: Phys. Rev. **40**, 749 (1932)
14 B. Boashash: Proc. IEEE **80**, 520 (1992); B. Boashash: Proc. IEEE **80**, 540 (1992)
15 L. Cohen: *Time–Frequency Analysis* (Prentice Hall, Englewood Cliffs, NJ 1995) Chapt. 8
16 Y.H. Cha, Y.I. Kang, C.H. Nam: J. Opt. Soc. Am. B **16**, 1220 (1999)